10 MAI 1983

TRI-PP-83-8
Feb 1983

Two-body form factors at high Q^2

Franz Gross
Department of Physics, College of William and Mary,
Williamsburg, Virginia 23185

B.D. Keister
Department of Physics, Carnegie-Mellon University,
Pittsburgh, Pennsylvania 15213

Abstract

The charge form factor of a scalar deuteron at high momentum transfer is examined in a model employing scalar nucleons and mesons. With an eye toward establishing consistency criteria for more realistic calculations, several aspects of the model are examined in detail: the role of nucleon and meson singularities in the one-loop impulse diagram, the role of positive- and negative-energy nucleons, and the relationship to time-ordered perturbation theory. It is found that at large Q^2 (1) the form factor is dominated by a term in which the spectator nucleon is on the mass shell, and (2) the meson singularity structure of the d-n-p vertex function is unimportant in determining the overall high-Q^2 behavior of the form factor.

(submitted to Physical Review C)

CERN LIBRARIES, GENEVA

I. INTRODUCTION

The deuteron is usually the first testing ground for a microscopic theory of short-distance phenomena in the nucleus. In particular, it is now very desirable to understand the role of nucleon substructure in nuclei, by means of such processes as electron-deuteron scattering at high Q^2. If nucleon substructure is controlled by quarks interacting via quantum chromodynamics, can these effects be described simply by including hadronic form factors in a conventional calculation with nucleons and mesons, or are there additional effects such as those of hidden color states which must be added to describe the data?

Indirect evidence for explicit substructure effects exists when a conventional theory involving nucleons and mesons fails to describe the data. Of course, such a theory must be internally consistent before any meaningful conclusions can be made by comparing to experiment. It is our view that any conventional calculation involving nucleons and mesons for $Q^2 > 1$ GeV^2 should be consistent with the asymptotic Q^2 behavior implied by the theory upon which it is based.

The purpose of this paper is to understand how to extract the asymptotic Q^2 behavior of electron scattering from a deuteron composed of scalar nucleons exchanging scalar mesons, with an eye toward understanding what approximations can or cannot be made which are consistent with this asymptotic behavior. We believe that even this simple model supplies most of the criteria needed for evaluating more realistic calculations.

The question of theoretical consistency is already an important one. Recent calculations by Zuilhof and Tjon,[1] using solutions to a Bethe-Salpeter equation, as well as results of Arnold, Carlson and Gross,[2]

using a covariant three-dimensional wave equation, agree approximately with each other, but fall substantially below recent SLAC elastic e-D data.[3]

However, in another approach, Gurvitz[4] achieves a fit to data up to $Q^2 = 6$ GeV^2, in which he claims to have included important Lorentz boost effects, as well as relevant meson singularities associated with the Bethe-Salpeter equation. The implied asymptotic behavior of each of these three calculations is also quite different: Gurvitz's approach, for example, gives a much slower asymptotic falloff than those of the other authors. Since all of these calculations involve similar physics, the discrepancy is a matter of theoretical self-consistency which must be resolved. This problem is addressed below, where we examine the asymptotic behavior implied by these different approaches.

The outline of this paper is as follows. First, the integral for the charge form factor in impulse approximation is written using the scalar model of nucleons and mesons. Then, the roles of all positive- and negative-energy nucleon poles are examined. If point-like deuteron vertices are assumed, the loop integral can be done exactly using light-cone perturbation theory. In this case, we find that the leading large-Q^2 behavior is also reproduced by a three-dimensional loop integral in which the spectator nucleon is placed on the mass shell. Following this, the structure of the deuteron vertex function is examined, with particular regard to the role of meson singularities. We find that the kinematic region in the vicinity of these singularities does not contribute to the leading large-Q^2 behavior. Finally, we discuss several realistic calculations of the deuteron charge form factor in terms of these model results.

II. ANALYSIS OF THE FORM FACTOR INTEGRAL

A. Description of the model

We consider a model deuteron of mass M_D composed of scalar nucleons of mass M, which exchange neutral scalar mesons of mass μ. We believe the neglect of spin to be reasonable here since we concentrate on the kinematic rather than structural aspects of the constituents. The effect of charged meson exchange currents can be added if one desires (see, however, Sec. II.C): this effect, together with a full treatment with spin, would would almost certainly be necessary before data could be fit.

Within this model, elastic e-D scattering is given by the Feynman diagram shown in Fig. 1. The deuteron charge form factor is

$$F_d(Q^2)(D+D')^\mu = -iF_N(Q^2)\int \frac{d^4k_1}{(2\pi)^4}\,\frac{\tilde{\Gamma}(k_1^2,k_2^2)(k_2+k_3)^\mu\,\tilde{\Gamma}(k_1^2,k_3^2)}{(M^2-k_1^2)(M^2-k_2^2)(M^2-k_3^2)}\,. \qquad (2.1)$$

Unless otherwise stated, we work in the Breit frame, where

$$D = (D_o, -\tfrac{1}{2}\vec{Q});\ D' = (D_o, +\tfrac{1}{2}\vec{Q});\ q = (0,\vec{Q});\ D_o = (M_d^2 + \tfrac{1}{4}Q^2)^{1/2}. \qquad (2.2)$$

$\tilde{\Gamma}(p_1^2,p_2^2)$ is an invariant d-n-p vertex function which depends upon the virtual nucleon masses p_1^2 and p_2^2. In principle, it is a solution to a Bethe-Salpeter equation involving the mesons in the theory. Its actual form will be specified below.

In this section we will emphasize the role of the singularities which come from the three nucleon propagators in (2.1). In particular, we will assume that the singularities of the vertex function $\tilde{\Gamma}$ are sufficiently distant so that they can be ignored (which would be the case if the "deuteron" were loosely bound by heavy mesons). The singularities of $\tilde{\Gamma}$ will be studied in the next subsection.

If the k_0 integration is performed by the method of residues, and the contour is closed in the lower half plane, then, as it was observed over 15 years ago,[5] the positive energy pole of the spectator dominates the form factor at low Q^2; the approximation in which only this pole is retained shall be referred to as the relativistic impulse approximation (RIA). It is a major purpose of this paper to show that this pole also dominates the expression (2.2) at large Q^2.

The six poles in the k_0 complex plane are located at

$$\begin{aligned} k_0 &= \pm(E_k - i\varepsilon) && (1^{\pm}) ; \\ k_0 &= D_0 \mp E_+ \pm i\varepsilon && (2^{\pm}) ; \\ k_0 &= D_0 \mp E_- \pm i\varepsilon && (3^{\pm}) , \end{aligned} \tag{2.3}$$

where

$$\begin{aligned} E_\pm &= \left[M^2 + \left(\vec{k} \pm \frac{1}{2}\vec{Q}\right)^2\right]^{1/2} ; \\ E_k &= \left[M^2 + k^2\right]^{1/2} \end{aligned} \tag{2.4}$$

and 1^+ (1^-) is the positive (negative) energy pole associated with particle 1 as labeled in Fig. 1, with similar notation for $2^\pm$ and $3^\pm$.

The location of the poles in the k_0 plane depends upon Q and the component of $\vec{k}$ parallel to $\vec{Q}$. It is convenient for later discussion to take $\vec{Q}$ along the y-axis. First, we consider the case when k_x and k_z are small. If $Q^2 \ll M^2$, the poles are as shown in Fig. 2(a). In this case, the pole at 1^+ nearly pinches the poles at 2^+ and 3^+ when k_y is small, and as k_y increases the poles in the lower half plane migrate toward the right, while those in the upper half plane migrate toward the left. If the k_0 integral is closed in the lower half plane, the singularity arising from the spectator being on its positive energy mass shell (1^+) will dominate, and the integrand of this term will be further dominated by small k_y values. These results lead to the conclusion that the RIA dominates at low Q^2, as discussed in Ref. 5.

If $Q^2 \gg M^2$, the poles change their position radically. Now we distinguish between two cases, according to whether the magnitude of k_y is larger or smaller than Q/2 ($|k_y| \gg M$ in both cases). If k_y is negative, these cases are shown in Figs. 2(b) and 2(c). When $-k_y$ is less than Q/2, the poles 1^+ and 2^+ pinch; as $-k_y$ becomes greater than Q/2, the 2^+ and 2^- poles are "reflected" at the Q/2 "boundary" and 1^+ and 2^- move as a double pole (they are on the same side of the complex plane). As a double pole, 1^+ and 2^- will nearly cancel, and hence the integrand will be large only when $-k_y < Q/2$, in which case it will be dominated by the spectator pole (1^+) as before. (If k_y is positive, the role of the $2^\pm$ vs. $3^\pm$ poles is reversed, but otherwise the analysis is the same.) If either k_x or k_z is not small, then the overall effect is to decrease the magnitude of the integral; specifically regarding the near-pinch singularity of Fig. 2(b), the 2^+ pole is moved to the left and the 1^+ pole to the right, thus reducing the strength of the near pinch. We conclude, therefore, that if the k_0 contour is closed in the lower half plane, then the integral for both low and high Q^2 is dominated by the positive energy spectator pole, whose residue is greatest where the nucleon momenta are co-linear.

The result of retaining the spectator pole in Eq. (2.1) is, for the μ=0 component,

$$F_d(Q^2) = F_N(Q^2) \int \frac{d^3k}{(2\pi)^3} \left(\frac{D_0 - E_k}{2D_0E_k}\right) \frac{\Gamma(k_2^2)\Gamma(k_3^2)}{(M^2-k_2^2)(M^2-k_2^2)} , \tag{2.5}$$

where we introduce the vertex function with one particle on shell

$$\Gamma(k_2^2) \equiv \tilde{\Gamma}(M^2,k_2^2) \ . \qquad (2.6)$$

Equation (2.5) can be shown to be nearly identical to the result one would obtain from light cone perturbation theory (LCPT).[6] To make the comparison, first add a term linear in k_z to the numerator of (2.5):

$$F_d(Q^2) = F_N(Q^2) \int \frac{d^3k}{(2\pi)^3} \left(\frac{D_o - E_k + k_z}{2D_o\ E_k}\right) \frac{\Gamma(k_2^2)\Gamma(k_3^2)}{(M^2-k_2^2)(M^2-k_3^2)} \ . \qquad (2.7)$$

(This expression is actually identical to Eq. (2.5) because the integrand of the new term linear in k_z is odd, so the extra term is zero.) Then introduce the transformation

$$x = \frac{E_k - k_z}{D_o} \ , \qquad (2.8)$$

to eliminate the variable k_z. Introducing $\vec{k}_\perp = (k_x,k_y)$, the transformed form factor is then

$$F_d(Q^2) = F_N(Q^2) \int \frac{d^2k_\perp}{2(2\pi)^3} \int_0^\infty \frac{dx}{x}\,(1-x)\, \frac{\Gamma(k_2^2)\Gamma(k_3^2)}{(M^2-k_2^2)(M^2-k_3^2)} \ , \qquad (2.9)$$

where

$$M^2 - k_{2,3}^2 = \frac{1}{x}\left[M^2 - x(1-x)M_d^2 + \left(\vec{k}_\perp \pm x\vec{Q}/2\right)^2\right] . \qquad (2.10)$$

If one were to evaluate the diagram of Fig. 1 using LCPT, a result identical to Eq. (2.9) would emerge, with the only difference being that the range of x integration is from zero to one. For LCPT, the variable x is defined as

$$x \equiv \frac{k_o + k_z}{D_o + D_z} \ , \qquad (2.8')$$

in place of Eq. (2.8).

If the vertex function is a constant, then the LCPT result is exact for the triangle. Hence the RIA errs by including the region x>1. From the viewpoint of the location of nucleon singularities discussed in Fig. 2, the large x region presumably corresponds to places where the 1^+ pole overlaps with either the 3^- or 2^- poles (and would be cancelled in

an exact calculation), as discussed above, so we can understand why this region should not be counted. However, as we show in detail in the Appendix, the results at low Q^2 and high Q^2 are not greatly affected by this error. This is because, for weakly bound systems, the form factor is dominated both at high and at low Q^2 by the region near $x = 1/2$ ($\vec{k}$ small). Hence the region for x>1 does not make significant contributions in either case, and the leading contributions at both low and high Q^2 are identical for the two models (see the Appendix).

In addition to the dominant power law dependence, there is also a log Q^2 contribution which comes from the region near x=0. These "end point singularities" have been previously discussed by Brodsky and Farrar,[7] and by Brodsky and Lepage.[8] In our example, a spinless ϕ^3 theory, they give a negligible contribution for all large (but finite) Q^2. (This is demonstrated in the Appendix for the special case where Γ is a triple pole.) Hence we will ignore such contributions from the end points in this paper, and consider the integral to be dominated by contributions from the region where the relative momentum of either the initial or final state is small.

The fact that the LCPT gives the exact result when the vertex function is a constant could be regarded as a strong reason for preferring it. However, when applying a relativistic formalism to a meson theory in nuclear physics, the vertex function will never be constant. Furthermore, the vertex function is in turn the solution of a bound state integral equation. For LCPT, this is usually the Weinberg equation,[6,9] in which a field theory is truncated to a fixed number of particles viewed from the light cone. Neither this approach nor the RIA will give exact results for the vertex function or the charge form factor. Hence, it may be more

important to choose a formalism which retains spherical symmetry and an easily interpreted non-relativistic limit. In this regard, the RIA is clearly superior to the Weinberg equation, and we regard the fact that they give the same results at high Q^2 to be an important, and somewhat unexpected, additional advantage of the RIA. Frankfurt and Strikman[10] have also compared these two approaches. They argue that there are substantial differences, but they never make a direct comparison, such as that based upon Eq. (2.9), which shows that the leading large-Q^2 results are the same.

It is useful to develop the RIA formalism further. We introduce positive and negative energy wave functions in a manner similar to that previously done for spin 1/2 constituents,[11]

$$\psi^+(k) = \frac{\Gamma(k_o^2)}{(2\pi)^{3/2}(2M_d)^{1/2}\ 2E_k[2E_k-M_d]}$$

$$\psi^-(k) = \frac{\Gamma(k_o^2)}{(2\pi)^{3/2}(2M_d)^{1/2}\ 2E_k\ M_d}\ . \qquad (2.11)$$

Then the form factor (2.5) at $Q^2=0$, which is equivalent to the relativistic normalization condition, becomes simply

$$1 = \int d^3k \left\{ |\psi^+(k)|^2 - |\psi^-(k)|^2 \right\}, \qquad (2.12)$$

which is a result familiar from the two-component form of the Klein-Gordon theory. The fact that the norm is not positive definite is to be expected for a Klein-Gordon theory.

The general result (2.5) can also be written in terms of the wave functions (2.11). We follow the techniques in Ref. 2, and boost the relativistic wave functions $\psi = \psi^+ + \psi^-$ to their rest system (which is trivial here because $k^2_{2,3}$ are invariants). The rest system three-vector momenta

$\vec{p}^{(2)}$ and $\vec{p}^{(3)}$ become

$$p_{x,z}^{(2,3)} = -k_{x,z}$$

$$p_y^{(2,3)} = -\frac{1}{M_d}\left(k_y\ D_o \pm \frac{1}{2}\ Q\ E_k\right). \qquad (2.13)$$

[See Eq. (2.52) of the second paper of Ref. 2.] In terms of these variables, and the energies $e_i = (M^2+p^{(i)2})^{1/2}$, we can write

$$F_d(Q^2) = F_N(Q^2)\ \frac{M_d}{D_o} \int d^3k \left\{ \theta_+(\psi_2^+\psi_3^+ - \psi_2^-\psi_3^-) + \theta_-(\psi_2^+\psi_3^- - \psi_2^-\psi_3^+) \right\}, \qquad (2.14)$$

where

$$\theta_+ = \left(\frac{D_o-E_k}{E_k}\right) \frac{M_d(e_2+e_3) - 2e_2e_3}{2(M_d-e_2)(M_d-e_3)}$$

$$\theta_- = \left(\frac{D_o-E_k}{E_k}\right) \frac{M_d(e_2-e_3)}{2(M_d-e_2)(M_d-e_3)}\ . \qquad (2.15)$$

Equation (2.14) reduces immediately to (2.12) when $Q\to 0$. At high Q^2, the leading contribution comes when either $\vec{p}^{(2)}$ or $\vec{p}^{(3)}$ are near zero, so that ψ^+ peaks sharply. It is sufficient to study either one of these points and multiply by two. When $\vec{p}^{(2)}=0$,

$$k_{x,z} = 0$$

$$k_y = -1/4\ Q$$

$$p_y^{(3)} \cong M + \frac{Q^2}{8M} = e_3 \qquad (2.16)$$

and (2.14) reduces to

$$F_d(Q^2) \xrightarrow[Q^2\to\infty]{} F_N(Q^2)\left(\frac{8M}{Q}\right)\psi\left(\frac{Q^2}{8M}\right) \int d^3k\ \psi^+(p_2)\ , \qquad (2.17)$$

where $\vec{p}^{(2)}$ has been set to zero everywhere except in ψ_2^+, the rapidly varying part. Equation (2.17) can be further reduced by noting that

$$\frac{dk_y}{dp_y^{(2)}} = \frac{E_k}{e_2} \xrightarrow[Q\to\infty]{p^{(2)}\to 0} \frac{Q}{4M} \qquad (2.18)$$

and defining the position space wave function by

$$\bar{\psi}(r) = \int \frac{d^3k}{(2\pi)^{3/2}} e^{i\vec{k}\cdot\vec{r}} \psi(k) . \qquad (2.19)$$

This gives finally

$$F_d(Q^2) \xrightarrow[Q\to\infty]{} F_N(Q^2)\ 2(2\pi)^{3/2}\ \tilde{\psi}^+(0)\psi^+\left(\frac{Q^2}{8M}\right) . \qquad (2.20)$$

We see that the asymptotic behavior of the body form factor depends on the product of the relativistic wave function at high momentum and the positive energy wave function at the origin. Since the wave function at large momentum depends entirely on the dynamics, Eq. (2.20) is not very helpful, and we will obtain a more useful relation in the next subsection.

B. The role of meson singularities

In the previous subsection it ws shown that the asymptotic form factor is dominated by contributions in which one wave function has low relative momentum and the other has high relative momentum. This result was summarized in Eq. (2.20). In this subsection we will complete the derivation of the asymptotic form factor by expressing the wave function at large momentum in terms of known quantities. In the process we will also examine the effect of the structure of the vertex function, neglected in the last subsection. The line of reasoning will be quite similar to that of Brodsky and Farrar.[7]

We begin by assuming that the bound state is held together by an infinite (ladder) sum of exchanges of a meson with mass μ. In this case, the form factor integrand in the region where $\vec{k} \approx -1/4\ \vec{Q}$ (low relative momentum for the initial wave function) is better described by the diagram in Fig. 3(a) which can be regarded as equivalent to Fig. 1, but with the structure of the final vertex function revealed so that its high momentum behavior can be studied. (If we wished to study the form factor in the region where $\vec{k} \approx 1/4\ \vec{Q}$, we would use Fig. 3(b). The contributions

from these diagrams are equal and the total result is twice either.)

Figure 3 gives:

$$F_d(Q^2) \approx -\frac{F_N(Q^2)}{2D_o}\int \frac{d^4k_1\ d^4k_1'}{(2\pi)^8} \times \frac{\tilde{\Gamma}(k_1^2,k_2^2)2(D_o-k_o)g^2\ \tilde{\Gamma}(k_3'^2,k_1'^2)}{(M^2-k_1^2)(M^2-k_2^2)(M^2-k_3^2)[\mu^2-(k_1-k_1')^2](M^2-k_3'^2)(M^2-k_1'^2)} . \qquad (2.21)$$

We first wish to examine the role of the explicit singularities which come from the meson propagator $\mu^2\sim(k_1-k_1')^2$. For this purpose, the k_1^o integration contour is closed in the lower half plane, where we know that it is safe to neglect the negative energy nucleon poles. Also, we will assume that the important singularities in $\tilde{\Gamma}$ have been included by keeping the meson pole; the additional singularities will also be neglected. This gives

$$F\ (Q^2) \approx -\frac{F_N(Q^2)}{2D_o}\int \frac{d^4k_1 d^4k_1'}{(2\pi)^8}\ \frac{\Gamma^2\ 2g^2(D_o-k_o)}{32\ E_kE_k'E_+E_-E_-'}\left(\frac{1}{2\omega}\right)\left[\frac{1}{\omega-k_o+k_o'-i\varepsilon}+\frac{1}{\omega+k_o-k_o'-i\varepsilon}\right] \times \left[\frac{1}{(E_k-k_o-i\varepsilon)(E_+-D_o+k_o-i\varepsilon)(E_--D_o+k_o-i\varepsilon)(E_k'-k_o'-i\varepsilon)(E_-'-D_o+k_o'-i\varepsilon)}\right] \qquad (2.22)$$

where the meson propagator is factored into two terms, and

$$\omega = \left[\mu^2 + (\vec{k}-\vec{k}')^2\right]^{1/2} . \qquad (2.23)$$

The reader can easily convince himself that the $k_1^{o\prime}$ integral can be closed in either half plane without overlapping any negative energy poles, and in both cases peaks at $\vec{k}' = 1/4\ \vec{Q}$. To simplify the algebra, the k_o' contour will always be closed so as to avoid the meson poles - in the lower half plane for the first term and in the upper half plane for the second. However, the k_1^o integral must always be closed in the lower half plane - and hence the first meson pole gives an explicit contribution. Introducing the notation

$$\sum = \frac{F_N(Q^2)}{2D_o} \int \frac{d^3k\ d^3k'}{(2\pi)^6} \frac{\Gamma^2\ 2g^2}{32\ E_k E_k' E_+ E_- E_-'} \frac{1}{2\omega} \tag{2.24}$$

there are three terms:

$$F_d(Q^2) = \sum \left\{ \frac{D_o - E_k}{(E_+ + E_k - D_o)(E_- + E_k - D_o)(E_-' + E_k' - D_o)(\omega + E_k' - E_k)} \right.$$

$$+ \frac{D_o - \omega - E_{k'}}{(E_k - \omega - E_{k'})(E_+ + \omega + E_{k'} - D_o)(E_- + \omega + E_{k'} - D_o)(E_-' + E_{k'} - D_o)}$$

$$\left. + \frac{D_o - E_k}{(E_+ + E_k - D_o)(E_- + E_k - D_o)(E_{k'} + E_-' - D_o)(\omega + E_k + E_-' - D_o)} \right\} . \tag{2.25}$$

Evaluating the three terms in braces at the peak $\vec{k} = -1/4\ \vec{Q}$ and $\vec{k}' = 1/4\ \vec{Q}$, and letting $Q \to \infty$, gives

$$\left\{ \right\} \xrightarrow[Q\to\infty]{} \left\{ \frac{Q}{16\alpha^4} + \frac{1}{4\alpha^2 Q} + \frac{Q}{16\alpha^4} \right\} , \tag{2.26}$$

where $\alpha^2 = ME$. We see that the meson pole terms are suppressed by a factor of $2\alpha^2/Q^2$, which guarantees that they are completely negligible. (A similar result at low momentum transfer was obtained in the first paper of Ref. 5.)

We have thus established that the structure of the vertex functions does not alter the validity of the basic result (2.20). The remainder of this section will be devoted to an improved evaluation of the aymptotic form factor using (2.21). Closing both the k_1^o and $k_1^{o\prime}$ contours in the lower half plane, and neglecting the meson poles, gives

$$F_d(Q^2) = \frac{F_N(Q^2)}{2D_o} \int \frac{d^3k\ d^3k'}{(2\pi)^6} \frac{\Gamma(k_2^2)}{2E_k(M^2 - k_2^2)} \frac{\Gamma(k_3'^2)}{2E_k'(M^2 - k_3'^2)} I , \tag{2.27}$$

where I is the Feynman diagram shown in Fig. 4(a). Equation (2.27) has a form ideal for further approximation. We view I as a slowly varying function of k and k', and evaluate it at the peak, $\vec{k} = -1/4\ \vec{Q}$ and $\vec{k}' = 1/4\ \vec{Q}$, which is equivalent to the diagram factorization illustrated in

Fig. 4, where

$$p = \left(E_o, -\frac{1}{4}\vec{Q} \right)$$

$$p' = \left(E_o, \frac{1}{4}\vec{Q} \right)$$

$$E_o = \left(M^2 + \frac{1}{16} Q^2 \right)^{1/2} . \tag{2.28}$$

Then, using Eqs. (2.18) and (2.19), and multiplying by 2 to include both Fig. 3(a) and 3(b):

$$F_d(Q^2) \underset{Q\to\infty}{=} 2F_N(Q^2) \frac{[\tilde{\psi}^+(0)]^2}{M_d D_o} \bar{I} , \tag{2.29}$$

where $\bar{I}$ is the value of I at the peaks, corresponding to Figs. 4(a) and 4(b). Specifically,

$$\bar{I} = \frac{g^2\ 2(D_o - E_o) F_{\mu NN}^2(-Q^2/4)}{1/2Q^2[\mu^2 + 1/4Q^2]} \simeq \frac{2D_o\ g^2}{Q^2[\mu^2 + Q^2/4]} \cdot \left[\frac{m_o^2 - \mu^2}{m_o^2 + Q^2/4} \right]^{2n} , \tag{2.30}$$

where $F_{\mu NN}(p^2)$ is the meson-nucleon form factor. Combining (2.29) and (2.30) yields the final result for spinless particles

$$F_d(Q^2) \underset{Q\to\infty}{=} \frac{F_N(Q^2)\ 2g^2[\tilde{\psi}^+(0)]^2}{M\ Q^2[\mu^2 + Q^2/4]} \cdot \left[\frac{m_o^2 - \mu^2}{m_o^2 + Q^2/4} \right]^{2n} . \tag{2.31}$$

The body form factor falls as $Q^{-(4+2n)}$ at large Q^2.

If n=0, this result is consistent with the work of Brodsky and Lepage,[8] who obtain Q^{-2} for two point-like constituents with a scale invariant interaction. Our interaction is not scale invariant; g has dimensions of mass, so the extra Q^{-2} is required to cancel the dimensions of g^2. This point was also addressed by Brodsky and Farrar.[7]

Comparison of Eqs. (2.20) and (2.31) suggests that

$$\psi\left(\frac{Q^2}{8M} \right) \xrightarrow[Q\to\infty]{} \frac{4g^2\ \tilde{\psi}^+(0)}{(2\pi)^{3/2}\ M\ Q^4} \cdot \left[\frac{4(m_o^2 - \mu^2)}{Q^2} \right]^{2n} . \tag{2.32}$$

This result can also be obtained directly from the relativistic wave

equation for ψ, which can be written

$$\psi(k) = \frac{1}{M_d(2E_k - M_d)} \int \frac{d^3k'}{(2\pi)^3} \frac{g^2 F^2_{\mu NN}[(E_k - E_{k'})^2 - (\vec{k} - \vec{k}')^2]}{\mu^2 + (k-k')^2 - (E_k - E'_k)^2} \frac{\psi(k')}{2E'_k}$$

$$\equiv \frac{g^2 \tilde{\psi}(0) F^2_{\mu NN}(2M^2 - 2ME_k)}{8M^2(E_k - M)[\mu^2 + k^2 - (E_k - M)^2] (2\pi)^{3/2}} . \qquad (2.33)$$

substituting $k = Q^2/8M$ into (2.33) gives (2.32) if terms involving μ^2/Q^2 are dropped.

The appearance of the wave function at the origin in these equations is a natural outcome of factorizing the momentum loop integral into a soft component [containing $\tilde{\psi}(0)$] and a hard component (containing the explicit meson propagation) which carries the high momentum transfer. For QCD calculations of hadron form factors,[8] $\tilde{\psi}(0)$ is treated as a phenomenological normalization constant. For a deuteron composed of nucleons and mesons, one could imagine doing the same thing, but there is a serious problem because $\tilde{\psi}(0)$ is intertwined with the short-range repulsion of the nucleon-nucleon force. Strictly speaking, our results always apply to a region of Q^2 which <u>exceeds</u> the mass of the heaviest meson exchanged, wherein $\psi(r)$ is slowly varying over the region $r < 1/Q$. Whether a real deuteron can ever be described by meson exchanges with a maximum mass (a possibility that is certainly <u>not</u> obvious from the staandpoint of QCD) is a dynamical question which is not addressed in this paper. Instead, our purpose is to examine the large-Q^2 behavior which is <u>implied</u> by current theories of the deuteron with a fixed number of meson-exchange potentials. Whether this large-Q^2 behavior agrees with experiment is a completely separate matter.

C. Other contributions

So far, we have considered the deuteron to be a bound-state solution to a ladder integral equation. Since the spectator is on its mass shell in our analysis, this condition can also be retained in the integral equation for the vertex function. In this case, the fourth-order kernel of the equation includes <u>both</u> the crossed-box diagram <u>and</u> that part of the full box not included when the second-order ladder kernel is iterated once (see Fig. 5).

It is useful to estimate the magnitude of these non-ladder contributions. We assume that the singularity analysis of Sec. II.A allows us again to factor out the deuteron wave function, leaving only the fourth-order kernel. We further assume that there are form factors at the meson-nucleon vertices to provide convergence. At the peak of the incoming wave function, when $\vec{p} = -\vec{Q}/4$, we see that three out of four denominators in the integrand of each diagram are small in the vicinity of $\ell^\mu = 0$. Indeed, if $\vec{\ell} = 0$ and $\vec{p} = -\vec{Q}/4$, then both nucleon poles in each diagram lie at $\ell_o = 0$. However, in this case there is a double pole, and not a pinch singularity. (The pinch singularity originally in the box diagram has already been included in the ladder sum; the part of the box with no pinch singularity is the only part remaining in the fourth-order kernel. An easy way to compute this piece is to move the singularity from the positive-energy spectator pole from the lower half plane to the upper half plane, where it combines with the singularity of the struck nucleon to form a double pole.) Because there is no pinch singularity, these diagrams are suppressed by a propagator derivative, leading to an extra power of $1/Q^2$. Furthermore, a detailed estimate of the two diagrams in Fig. 5 shows that their leading terms cancel for very high

Q^2, suppressing their contribution by still another power of $1/Q^2$. In higher-order kernels, diagrams with more crossed lines will have further pinch singularities of their uncrossed counterparts replaced by double poles, leading to further suppression. Thus, the meson ladder terms with on-shell spectators give the leading-Q^2 behavior. This result is similar to one obtained for the relativistic eikonal expansion of nucleon-nucleon scattering, in which the leading contribution to the eikonal phase is correctly summed by including only the ladder terms with on-shell spectator nucleons.[12]

Without going into detail, we can also estimate the contribution from meson exchange currents (MEC). Following factorization, some lower-order diagrams are shown in Fig. 6. For the charged MEC, Fig. 6(a), the momentum transfer is shared by the meson propagators with Q/2 apiece, as compared to Fig. 4, in which a nucleon carries momentum q and a meson momentum q/2. However, in this case, the energy carried by the mesons is zero. Because the energy factor is in the numerator, this diagram is zero at the peak, suppressing its contribution, which would otherwise compete with the leading terms in the ladder sum. The contributions from the two-meson MEC diagrams shown in Figs. 6(b) and 6(c) are suppressed in a way similar to their counterparts shown in Fig. 5. They also cancel each other at the peak.

We conclude that, for a spinless theory, the ladder sum with on-shell spectators dominates at high Q^2 over higher-order kernels and MEC.

D. The role of time-ordered diagrams

If the factorization of the deuteron form factor integral is correct, then it is quite simple to analyze the contributions from various time-ordered diagrams. The factorized charge form factor has two

identical contributions, as shown in Figs. 4(a) and 4(b), where all four external lines are on the mass shell. The amplitude for this diagram is $F_N(Q^2)g^2 \cdot 4/Q^3$, as $Q^2 \to \infty$ in the Breit frame. (The extra factor of Q comes from the factor of $2D_0$ - recall Eq. (2.11).)

We now examine the first of these two Feynman diagrams in terms of time-ordered perturbation theory in the Breit frame, by decomposing the nucleon and meson propagators. In this subsection, the meson-nucleon form factors are set to unity. The invariant amplitude is $\mathcal{M}(Q^2) = F_N(Q^2)[I^{(+)}(Q^2) + I^{(-)}(Q^2)]$, where the positive-energy part is

$$I^{(+)}(Q^2) = \frac{g^2(E_0+E')}{4\omega'E'}\left[\frac{1}{-\omega'(E_0-E')} + \frac{1}{(E_0-E')(E_0-E'-\omega')} + \frac{1}{-\omega'(E_0-E'-\omega')}\right], \tag{2.34}$$

where $E_0 = (Q^2/16+M^2)^{1/2}$; $E' = (4Q^2/16+M^2)^{1/2}$; $\omega' = (Q^2/4+\mu^2)^{1/2}$. The three terms follow the order of (+) diagrams (i), (ii), (iii) of Fig. 7. The negative-energy part is

$$I^{(-)}(Q^2) = \frac{g^2(E_0-E')}{4\omega'E'}\left[\frac{1}{-\omega'(-E_0-E')} + \frac{1}{(-E_0-E')(-E_0-E'-\omega')} + \frac{1}{-\omega'(-E_0-E'-\omega')}\right], \tag{2.35}$$

where the three terms follow the (-) diagrams of Fig. 7.

As $Q^2 \to \infty$, we find that

$$I^{(+)}(i) \to 8g^2/3Q^3;\ I^{(+)}(ii),\ I^{(+)}(iii) \to 4g^2/3Q^3;$$
$$I^{(-)}(i) \to 2g^2/3Q^3;\ I^{(-)}(ii) \to 2g^2/9Q^3;\ I^{(-)}(iii) \to 4g^2/9Q^3\ . \tag{2.36}$$

The positive-energy terms overestimate the full result, accounting for 4/3 of the total. This is not surprising, because the struck nucleon is very far off shell. It is also interesting to note that the so-called recoil term, $I^{(+)}(iii)$, which is suppressed at low Q^2, is comparable to the other terms at high Q^2, and that the recoil term cancels the sum of the negative-energy terms.

Of course, the relative strengths of different time-ordered diagrams are frame dependent. For example, in the infinite-momentum frame (equivalently, quantization on the light plane), the negative-energy terms vanish. Nevertheless, there remain three time-ordered terms in place of a single Feynman graph. Our view is that it is simplest in practice to retain the Feynman picture and perform any necessary loop integral directly, keeping the positive-energy spectator pole, rather than decomposing into a time-ordered or x^+-ordered framework.

III. COMPARISON WITH OTHER APPROACHES

On the basis of the analysis of the previous section, we are now in a position to understand some of the similarities and the differences between the various charge form factor calculations discussed in the Introduction.

In Sec. II.A and in the Appendix, we found that the four-dimensional loop integral for the charge form factor is dominated at large Q^2 by the positive-energy spectator pole, thus leaving a three-dimensional integral to do. Since the vertex functions Γ in the integrand are to be evaluated for various three-dimensional arguments, one can also compare the results of using a four-dimensional (Bethe-Salpeter) solution to those where Γ is a solution to a three-dimensional equation where each intermediate spectator nucleon is on the mass shell. The <u>difference</u> between using the three- or the four-dimensional solution in the form factor integral involves diagrams of the sort shown in Fig. 5(b). However, as shown in Sec. II.C, these differences are suppressed at large Q^2. Thus, we can see in a simple way why the calculated charge form factor is so similar between Arnold, Carlson and Gross,[2] who use three-dimensional equations, and Zuilhof and Tjon,[1] who use the Bethe-Salpeter equation directly.

We now turn to the calculations of Gurvitz and Bhalerao,[4] who obtained substantially different results from either Ref. 1 or 2, yet claim to have similar, if not improved, physical content in their theory. To understand their approach in terms of our notation, it is useful to write Eq. (2.14) in the approximation

$$\psi^- \ll \psi^+$$
$$\theta_- \ll \theta_+ \approx 1 \tag{3.1}$$

which gives

$$F_d(Q^2) = F_N(Q^2)\,\frac{M_d}{D_o}\int d^3k\ \psi_2^+\psi_3^+ \ . \tag{3.2}$$

This formula is a good approximation to (2.14) at low Q^2, and also has the same power law dependence at high Q^2 (although the normalization differs somewhat). Gurvitz and Bhalerao (GB) argue that each wave function in (3.2) should be replaced with one-half the sum of two terms, one in which the spectator is on shell, plus one in which the struck nucleon is on shell:

$$\psi_1^+ \to \frac{1}{2}\left(\psi_1^+ + \chi_1^+\right), \tag{3.3}$$

where χ^+ is obtained by transforming ψ as if the <u>struck</u> nucleon were on shell:

$$E_k^2 - (D_o - E_\pm)^2 = M_d\left(2E_t^{(2,3)} - M_d\right) \ , \tag{3.4}$$

where

$$t_{x,z}^{(2,3)} = -k_{x,z}$$
$$t_y^{(2,3)} = -\frac{1}{M_d}\left(k_y D_o \pm \frac{Q}{2}\left[D_o - E_\pm\right]\right), \tag{3.5}$$

and $E_\pm$ were defined in Eq. (2.4). Hence χ_1^+ is identical to (2.11) with $\vec{k}$ replaced by (3.5) instead of (2.13).

We believe that the GB prescription (3.3) cannot be derived from meson field theory in the way claimed by the authors, and must be

regarded as ad hoc. To prove this, it is sufficient to look at the integrand of Eq. (3.2) near the peak of the initial bound state wave function, as was done in Sec. II.A following Eq. (2.16). Both $p^{(2)}$ and $t^{(2)}$ are small when $k_{x,z} \simeq 0$ and $k_y = -1/4\ Q$, and the large Q behavior of the form factor will depend, as before, on the behavior of the outgoing wave function. While $p^{(3)}$ is large as $Q\to\infty$, as given in Eq. (2.16), $t^{(3)}$ approaches a constant

$$t^{(3)} \xrightarrow[Q\to\infty]{k_y=-1/4Q} \frac{4}{3} M \ . \tag{3.5}$$

This behavior means that the GB body form factor approaches a constant asymptotically, regardless of the high momentum behavior of ψ!

As the preceding example shows, the dominant part of the GB form factor comes from a region where both the relative momentum of the incoming (outgoing) wave function is small, and the struck nucleon of the outgoing (incoming) wave function is on shell. However, such a kinematic region does not exist! In qualitative terms, it corresponds to a configuration of nucleons in which there is no way for the large momentum transfer Q to be distributed between them. A quantitative understanding of this result and the reason it is incorrect relies upon the singularity analysis of Sec. II.A, which we now develop in more detail.

First, we examine Fig. 2(b), which shows the singularities of the integrand when $k_y \simeq -1/4\ Q$, $Q \gg M^2$. In order that the initial wave function have low relative momentum, the relative energy must also be zero, which is possible if and only if we close the contour in the lower half plane and retain the 2^+ pole, or close the contour in the upper half plane and retain the 2^+ pole. Both procedures give essentially the same result, and in both cases the struck nucleon is far off shell. If we

insisted on placing the outgoing struck nucleon on its positive energy mass shell, we would need to retain the 3^+ pole, which would mean that the relative energy of the initial wave function was no longer small! Even if we ignore this last point, retaining the 3^+ pole only is guaranteed to give an error, because in this kinematic situation Fig. 2(b) shows that the 3^+ and 1^- poles are very close, and a completely wrong answer is obtained by keeping one and ignoring the other.

This last point will be illustrated quantitatively. Suppose we consider the propagators of particles 1 and 3 only, ignoring particle 2. Then retaining the 3^+ pole only is equivalent to the following calculation

$$\begin{aligned} J &\equiv -2\pi i \int \frac{dk_o\ \Gamma_o}{(E_k^2-k_o^2-i\epsilon)(E_-^2-(D_o-k_o)^2-i\epsilon)} \\ &= \frac{\Gamma_o}{2E_-\ M_d\left(2E_t^{(3)}-M_d\right)} \\ &= \frac{\Gamma_o}{4E_-\ E_t^{(3)}}\left(\frac{1}{2E_t^{(3)}-M_d}+\frac{1}{M_d}\right) \\ &\simeq \frac{\Gamma_o}{4E_-\ E_t^{(3)}}\left(\frac{1}{2E_t^{(3)}-M_d}\right) = \frac{\sqrt{2\pi^3(2M_d)}}{2E_-}\ \psi^+\left(t^{(3)}\right) . \end{aligned} \tag{3.6}$$

We are able to obtain the result (3.6) only by ignoring the 1^- pole. Furthermore, the fact that $t^{(3)}$ approaches a constant at large Q follows also from the proximity of the 1^- pole. Specifically,

$$\begin{aligned} \frac{1}{M_d\left(2E_t^{(3)}-M_d\right)} &= \frac{1}{E_k^2-(D_o-E_-)^2} = \frac{1}{(E_k+E_--D_o)(E_k-E_-+D_o)} \\ &\xrightarrow[Q\to\infty]{k_z=-1/4Q} \frac{1}{(Q/2)(16M^2/3Q)} \ . \end{aligned} \tag{3.7}$$

The second term in the denominator of (3.7) is the distance between the 3^+ and 1^- poles, and approaches zero when $k_y = -1/4Q$ and $Q \to \infty$, forcing the overall result to a constant.

The correct calculation requires that we keep both poles, which gives an extra term that cancels the bulk of (3.6). The correct evaluation gives

$$J = \frac{\Gamma_0}{2E_-\left(E_k^2-(D_0-E_-)^2\right)} + \frac{\Gamma_0}{2E_k\left(E_-^2-(D_0+E_k)^2\right)}$$

$$= \frac{\Gamma_0}{4E_kE_-}\left(\frac{1}{E_k+E_--D_0} + \frac{1}{E_k-E_-+D_0} + \frac{1}{E_-+E_k+D_0} + \frac{1}{E_--E_k-D_0}\right). \qquad (3.8)$$

The offending term $(E_k-E_-+D_0)^{-1}$ cancels, giving the asymptotic behavior:

$$J = \frac{\Gamma_0}{4E_kE_-}\left(\frac{1}{E_k+E_--D_0} + \frac{1}{E_-+E_k+D_0}\right)$$

$$\underset{Q\to\infty}{k_y=-1/4Q} \frac{\Gamma_0}{2E_-}\left(\frac{4}{Q^2} + \frac{4}{3Q^2}\right). \qquad (3.9)$$

When the propagator of particle 2 is included, the contribution from the near double $(3^+,1^-)$ pole is further suppressed and need not be considered at all!

The above discussion shows that the form (3.3) fails at high momentum transfer. It enhances the form factor in a completely artificial way. At lower momentum transfer, when $Q^2 \ll M^2$, the 3^+ pole does not overlap the 1^- pole, [see Fig. 2(a)]. Here a new problem arises due to the overlap of the 3^+ and 2^+ poles. For this reason it is also wrong to keep only the 2^+ pole. The uniform manner in which the 3^+ pole moves from the 2^+ pole to the 1^- pole as Q increases (for negative k_y) shows that it is inefficient to close the k_0 contour in the upper half plane. Closing the contour in the lower half plane and retaining the 1^+ pole only gives

a reliable approximation everywhere except at both high Q^2 and high $|k_y| > Q/2$, where the 1^+ and 3^- (or 2^-) poles overlap [Fig. 2(c)]. Fortunately, the region of high Q and high $|k_z|$ makes a negligible contribution to the form factor, so that this error is unimportant.

To summarize, we have shown that the dominant contribution to the deuteron charge form factor at high Q^2 is given by a three-momentum loop integral with the spectator nucleon on the mass shell. The leading behavior is the same as would be obtained in light-cone perturbation theory or in a calculation using the Bethe-Salpeter equation. In particular, we find that contributions from meson singularities, as well as charged meson currents, are not of leading order. Three-dimensional approaches in which non-spectator nucleons are placed on the mass shell must be handled carefully to avoid giving spurious results at high Q^2.

One of us (B.D.K.) wishes to thank the Theory Group at TRIUMF for their hospitality during a visit wherein this paper was completed. Both authors were supported in part by the U.S. National Science Foundation.

References

[1]M.J. Zuilhof and J.A. Tjon, Phys. Rev. C 22, 2369 (1980).

[2]R.G. Arnold, C.E. Carlson, and F. Gross, Phys. Rev. Lett. 38, 1516 (1977); Phys. Rev. C 21, 1426 (1980).

[3]R.G. Arnold et al., Phys. Rev. Lett. 35, 776 (1975).

[4]R.S. Bhalerao and S.A. Gurvitz, Phys. Rev. Lett. 47, 1815 (1981); S.A. Gurvitz, Weizmann Institute of Science report WIS-81/47 Oct-PH.

[5]F. Gross, Phys. Rev. 140, B410 (1965); 142, 1025 (1966); 152, 1517 (1966)E.

[6]S. Weinberg, Phys. Rev. 150, 1313 (1966); S.-J. Chang and S.-K. Ma, Phys. Rev. 180, 1506 (1967); J. Kogut and D. Soper, Phys. Rev. D 1, 2901 (1970); S.J. Brodsky, R. Roskies, and R. Suaya, Phys. Rev. D 8, 4574 (1973).

[7]S.J. Brodsky and G. Farrar, Phys. Rev. D 11, 1309 (1975).

[8]G.P. Lepage and S.J. Brodsky, Phys. Rev. D 22, 2157 (1980).

[9]J.M. Namyslowski and H.J. Weber, Z. Phys. A295, 219 (1980); B.L.G. Bakker, L.A. Kondratyuk and M.V. Terent'ev, Nucl. Phys. B158, 497 (1979).

[10]L.L. Frankfurt and M.I. Strikman, Nucl. Phys. B148, 107 (1979).

[11]W.W. Buck and F. Gross, Phys. Rev. D 20, 2361 (1979).

[12]S.J. Wallace, in Advances in Nuclear Physics, eds. J.W. Negele and E.W. Vogt, vol. 12 (Plenum, New York, 1981), p. 135; S.J. Wallace and J.A. McNeil, Phys. Rev. D 16, 3565 (1977).

APPENDIX

In this Appendix we estimate the high-Q^2 behavior of the form factor for a model in which the vertex function is approximated by a triple pole

$$\bar{\Gamma}(p_1^2,p_2^2) = \Gamma_0\left[\frac{2}{\Lambda^2-(p_1-p_2)^2}\right]^3 = \Gamma_0\left[\frac{2}{\Lambda^2+M_d^2-2p_1^2-2p_2^2}\right]^3 . \qquad (A.1)$$

In a realistic theory with nucleon structure, the vertex function is generated by a meson propagator and two meson-nucleon form factors. While the relevant masses are in general different, the use of a triple pole with a single mass is sufficient for studying the high-Q^2 behavior. If one particle is on shell, then

$$\Gamma(p^2) = \frac{\Gamma_0}{(M_\Lambda^2-p^2)^3} , \qquad (A.2)$$

where

$$M_\Lambda^2 = \frac{1}{2}\left(\Lambda^2+M_d^2\right) - M^2 \equiv \beta^2+M^2 . \qquad (A.2)$$

If Λ is some effective meson mass of the order of the pion mass, then $\beta^2 > 0$.

In what follows we will assume that the deuteron is loosely bound, and also that its significant structure is considerably larger than the Compton wave length of a nucleon. In terms of β^2 and $\alpha^2 = M^2 - 1/4M_d^2 = M\varepsilon$, this means that

$$\alpha^2 \ll M^2$$
$$\beta^2 \ll M^2 . \qquad (A.4)$$

(In realistic cases, $\alpha^2 \approx 0.002\ M^2$, and $\beta^2 \approx m_\pi^2 \approx 0.02\ M^2$, so these conditions are reasonably well satisfied.) For simplicity, we will also assume $\alpha^2 \ll \beta^2$, although this assumption is not essential.

Using the vertex function (A.2), the wave function $\psi = \psi^+ + \psi^-$ is

$$\psi(k) = \frac{\Gamma_o}{(2\pi)^{3/2}(2M_d)^{1/2}\, M_d(2E_k - M_d)\left[\beta^2 + M_d(2E_k - M_d)\right]^3}$$

$$\cong \frac{\Gamma_o x^4}{(2\pi)^{3/2}(2M_d)^{1/2}\, D(0,k_\perp) D^3(\beta^2,k_\perp)} , \qquad (A.5)$$

where

$$D(\beta^2,k_\perp) \equiv x\beta^2 + 4x(1-x)\alpha^2 + (1-2x)^2 M^2 + k_\perp^2 . \qquad (A.6)$$

Note that this wave function falls as k^{-4} as $k \to \infty$; the triple pole in (A.2) ensures that the quantity $\tilde{\psi}(0)$ is finite. It is sometimes convenient to write the wave function in the following form:

$$\psi(k) = \frac{\Gamma_o}{(2\pi)^{3/2}(2M_d)^{1/2}} \frac{x^2}{2} \frac{d^2}{dy^2} \frac{1}{y} \int_o^y dz\, \frac{1}{D^2(z,k_\perp)} \Bigg|_{y=\beta^2} . \qquad (A.7)$$

In this notation, the body form factor becomes

$$F_d(Q^2) = \frac{\Gamma_o^2}{2(2\pi)^3} \int d^2k_\perp \int_o^\lambda dx\, \frac{x^7(1-x)}{D(0,k_\perp) D(0,k_\perp+xQ) D^3(\beta^2,k_\perp) D^3(\beta^2,k_\perp+xQ)} , \qquad (A.8)$$

where $\lambda = 1$ for LCPT and $\lambda = \infty$ for the RIA. The constant Γ_o can be determined from the normalization condition, which for LCPT is

$$1 = \frac{\Gamma_o^2}{2(2\pi)^3} \int d^2k_\perp \int_o^1 dx\, \frac{x^7(1-x)}{D^2(0,k_\perp) D^6(\beta^2,k_\perp)} . \qquad (A.9)$$

This integral can be rewritten

$$1 = \frac{1}{5!} \frac{d^4}{dy^4} \frac{\Gamma_o^2}{2(2\pi)^3} \int d^2k_\perp \int_o^1 dx\, \frac{x^3(1-x)}{D^2(0,k_\perp) D^2(y,k_\perp)} \Bigg|_{y=\beta^2}$$

$$= \frac{1}{5!} \frac{d^4}{dy^4} \frac{\Gamma_o^2}{2(2\pi)^3} \int d^2k_\perp \int_o^1 dx\, \frac{x(1-x)}{y^2} \left(\frac{1}{D(0,k_\perp)} - \frac{1}{D(y,k_\perp)} \right)^2 \Bigg|_{y=\beta^2} \qquad (A.10)$$

If $\alpha \ll p$, the integral is dominated by the $D^{-2}(0,k_\perp)$ term, which can readily be integrated to give

$$1 = \frac{\Gamma_o^2}{8(16)\pi M\alpha\, \beta^{12}} . \qquad (A.11)$$

Hence, to $\mathcal{O}(\alpha^2/\beta^2)$,

$$\Gamma_o = 8\sqrt{2\pi M\alpha}\, \beta^6 . \qquad (A.12)$$

While this estimate (A.12) may not be very accurate if $\alpha \cong \beta$, the conditions (A.4) are sufficient to ensure that the difference between Γ_o obtained from LCPT and from the RIA is very small. This difference can be estimated from the difference in the normalization conditions, which is the region of integration $x > 1$. Specifically,

$$\frac{\Gamma_o^2}{2(2\pi)^3} \int d^2k_\perp \int_1^\infty dx\, \frac{x^7(1-x)}{D^2(0,k_\perp) D^6(\beta^2,k_\perp)} \cong \Gamma_o^2\, \mathcal{O}\left(\frac{1}{M^{14}}\right)$$

$$\cong \mathcal{O}\left(\frac{\alpha\beta^{12}}{M^{13}}\right) \ll 1 , \qquad (A.13)$$

where the estimate (A.12) is sufficiently accurate to show that this difference term is very small. It is completely negligible for the typical values of α and β given above.

We now examine the asymptotic behavior of the form factor (A.8). There are two objectives. One is to obtain the explicit asymptotic form and to investigate the size of the leading log Q^2 term; the other is to compare the results obtained from the RIA and from the LCPT.

In order to isolate the logarithmic term, we write the form factor as the sum of two quantities:

$$F_d(Q^2) = F_o(Q^2) + F_L(Q^2) , \qquad (A.14)$$

where, for LCPT,

$$F_L(Q^2) \equiv \frac{\Gamma_o^2}{2(2\pi)^3} \int d^2k_\perp \int_o^1 dx\, \frac{x^7}{(M^2+k_\perp^2)^4 \left[M^2 + (\vec{k}_\perp + x\vec{Q})^2\right]^4} , \qquad (A.15)$$

and

$$F_o(Q^2) \equiv F_d(Q^2) - F_L(Q^2) . \qquad (A.16)$$

The contribution F_L will be shown to fall as $Q^{-8}\log Q^2$ at large Q, while the F_0 term is regular as $x \to 0$ and consequently falls as Q^{-8}. The F_0 term is easy to estimate; because its integrand is regular at $x = 0$ the integral is dominated by contributions near the two regions $x = 1/2$ and $k_\perp = 0$, and $x = 1/2$ and $k_\perp = -1/2\ Q$. The contributions from both of these regions are equal, so that

$$F_0(Q^2) \xrightarrow[Q^2\to\infty]{} 2C_0/Q^8 \ , \tag{A.17}$$

where C_0 can be estimated from the region near $x = 1/2$, $k_\perp = 0$:

$$C_0 = \frac{\Gamma_0^2}{2(2\pi)^3}\int d^2k_\perp \int_0^1 \frac{dx}{x}\left\{\frac{1-x}{D(0,k_\perp)D^3(\beta k_\perp)} - \frac{1}{(M^2+k^2)^4}\right\}$$

$$\propto \frac{\Gamma_0^2}{2(2\pi)^3}\frac{1}{2}\frac{d^2}{dy^2}\frac{4}{y}\int_0^y dz \int d^2k_\perp \int_0^1 dx\ \frac{1}{D^2(z,k_\perp)}\bigg|_{y=\beta^2}, \tag{A.18}$$

where the first term in braces dominates at $x = 1/2$.

Before evaluating (A.18), we note that

$$\tilde\psi(0) = \int d^2k_\perp \int_0^1 \frac{dx\ M_d(1-x)\ \Gamma_0\ x^3}{(2\pi)^3\ (2M_d)^{1/2}\ D(0,k_\perp)\ D^3(\beta^2,k_\perp)}$$

$$= \frac{\sqrt{M}\Gamma_0}{(2\pi)^3}\frac{1}{2}\frac{d^2}{dy^2}\frac{1}{y}\int_0^y dz \int d^2k_\perp \int_0^1 \frac{x(1-x)}{D^2(z,k_\perp)}\bigg|_{y=\beta^2}. \tag{A.19}$$

Using the fact that (A.19) peaks at $x = 1/2$, and comparing with (A.18) gives

$$C_0 \simeq \frac{8\Gamma_0}{\sqrt{M}}\ \tilde\psi(0) \ . \tag{A.20}$$

Then, from (A.5) we have

$$\psi\left(\frac{Q^2}{8M}\right) \xrightarrow[Q\to\infty]{} \frac{16\Gamma_0}{(2\pi)^{3/2}(2M_d)^{1/2}\ Q^8} \ . \tag{A.21}$$

Combining (A.17), (A.20) and (A.21) gives

$$F_0(Q)^2 \xrightarrow[Q\to\infty]{} 2(2\pi)^{3/2}\ \psi\left(\frac{Q^2}{8M}\right)\tilde\psi(0) \tag{A.22}$$

in agreement with Eq. (2.20).

We now return to Eq. (A.18) in order to obtain an estimate of the size of C_0. First we perform the $k_\perp$ integration, and then extend the x integration from $-\infty$ to $+\infty$, introducing a small error which will be discussed below. Performing the x integration by the method of residues, and taking $\alpha \ll \beta$ for simplicity gives

$$C_0 \simeq \frac{\Gamma_0^2}{4\pi M}\ \frac{3\sqrt{2}}{8\beta^5} \ . \tag{A.23}$$

While this estimate is not very accurate if $\alpha \simeq \beta$, it is sufficient to draw the important conclusion that the contribution to C_0 from the region of x outside the interval $0 \leq x \leq 1$, which is of order M^{-6}, is completely negligible compared to that from within the interval $0 \leq x \leq 1$. Hence the leading Q^{-8} behavior of the form factor obtained from the RIA agrees with that obtained from LCPT to $\mathcal{O}(\beta^5/M^5)$, a negligible error for typical values of β.

Our last task is to evaluate the leading log behavior which comes from the region near $x = 0$ and is contained in F_L. To evaluate A.15), we use the fact that

$$\int_{-\infty}^{\infty} dk_y\ \frac{1}{(A^2+k_y^2)(A^2+(k_y+C)^2)^4}$$

$$\xrightarrow[C\to\infty]{} \frac{5\pi}{8A^7}\left[\frac{1+\mathcal{O}(A^2/C^2)}{(C^2+4A^2)^4} + \mathcal{O}\left(\frac{A^2}{(C^2+4A^2)^5}\right)\right] . \tag{A.24}$$

Neither of the two correction terms in (A.24) contribute to leading order, which is $Q^{-8}\log Q^2$, and are thus ignored. Setting $\alpha = 0$, we find that

$$F_L(Q^2) \underset{Q\to\infty}{} \frac{5\Gamma_o^2}{128\pi^2}\int_{-\infty}^{\infty} dk_x \int_0^1 \frac{dx}{x} \frac{1}{(M^2+k_x^2)^{7/2}[Q^8+(16(M^2+k_x^2)Q^6)/x^2]}$$

$$= \frac{5\Gamma_o^2}{(16\pi)^2 Q^8}\int_{-\infty}^{\infty} \frac{dk_x}{(M^2+k_x^2)^{7/2}} \log\left(\frac{Q^2}{16(M^2+k_x^2)}\right)$$

$$\simeq \frac{\Gamma_o^2}{48\pi^2 M^6 Q^8} \log (Q^2/16M^2) \ . \qquad (A.25)$$

The ratio of the log term to the leading Q^{-8} term is roughly

$$\frac{F_L}{F_o} \simeq \frac{1}{9\pi\sqrt{2}} \frac{\beta^5}{M^5} \log\left(\frac{Q^2}{16M^2}\right) . \qquad (A.26)$$

For the typical numbers we have been using, note that F_L does not become comparable to F_o until

$$Q^2 \simeq 16M^2 \, e^{9\pi\sqrt{2}\, M^5/\beta^5} \simeq M^2 \, 10^{3.1\times 10^5} \ , \qquad (A.27)$$

which is a ridiculously large value of Q^2. Hence, for practical purposes the log Q^2 term is negligible, and the form factor may be regarded as decreasing as a power of Q^2 (Q^{-8} in this case). As in the above cases, the coefficients of the log Q^2 term obtained from the RIA and LCPT are equal to a high accuracy.

We conclude that both the low and high Q^2 limits of the form factor are dominated by contributions of x near 1/2, and hence the RIA and LCPT give the same results to high accuracy. Furthermore, the log Q^2 behavior is also negligible for all values of Q^2 likely to be reached in any experiment.

Figure Captions

1. The relativistic impulse approximation to elastic electron-deuteron scattering, illustrating the kinematics used in the text. An "x" on a line denotes a particle on the mass shell.
2. Location of the poles of the k_o integrated for electron-deuteron scattering in the Breit frame. Configurations are shown for three different ranges of k_y. The arrows indicate the motion of the five poles for increasing k_y.
3. The Feynman diagram for electron-deuteron scattering with a single meson exchange exposed by iterating the bound-state equation for (a) the final deuteron and (b) the initial deuteron.
4. Factorization of the invariant electron-deuteron amplitude into mass-shell Feynman diagrams.
5. The contribution of the fourth-order kernel to the factorized electron-deuteron amplitude: (a) crossed-box; (b) subtracted-box (the circle on the line means that everything except the on-shell pole is retained).
6. Meson exchange current contributions to the factorized electron-deuteron amplitude: (a) charged-meson; (b) crossed-box; (c) subtracted-box, the latter two comprising part of the two-meson-exchange contributions.
7. Decomposition of the one-pion-exchange Feynman diagram into positive- and negative-energy time-ordered diagrams.

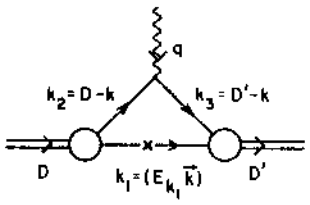

Fig. 1

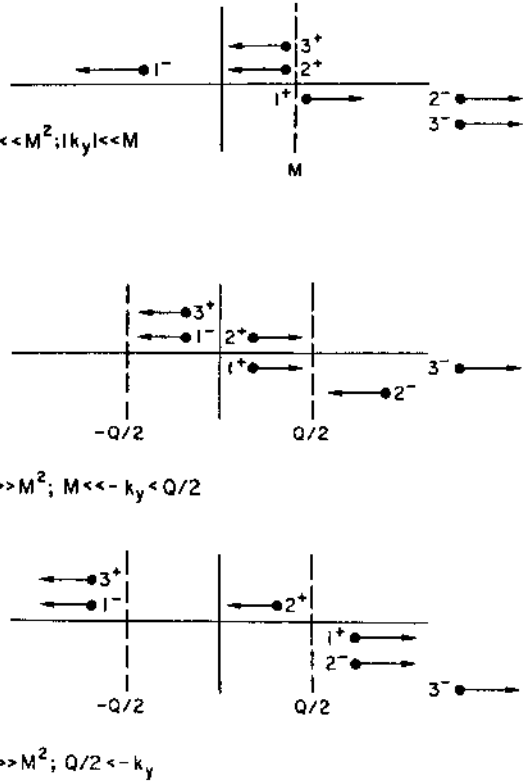

Fig. 2

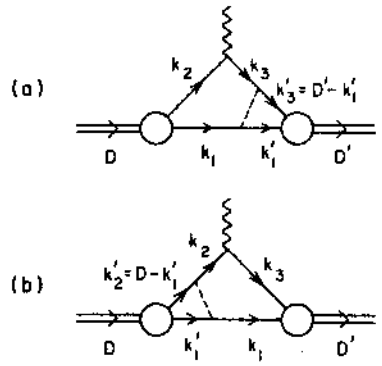

Fig. 3

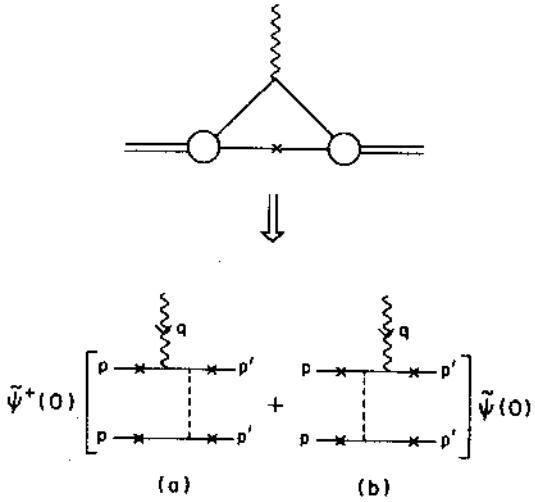

Fig. 4

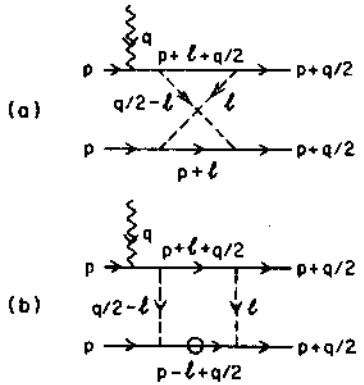

Fig. 5

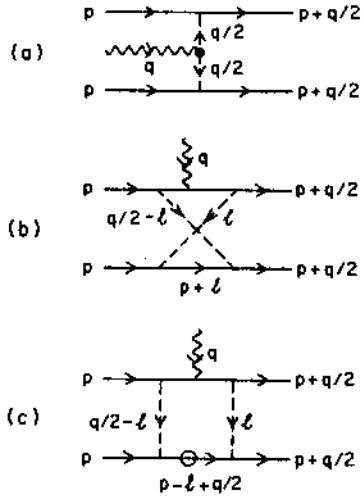

Fig. 6

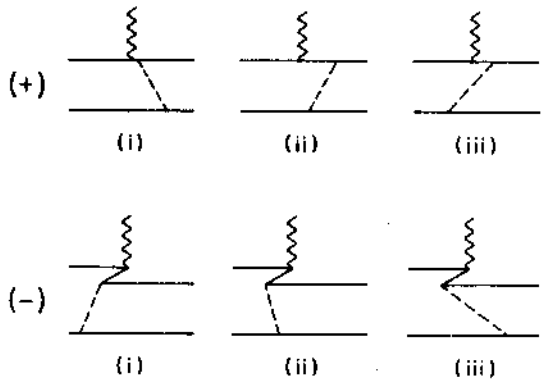

Fig. 7